Rare Metal Materials and Engineering
Volume 53, Issue 2, February 2024
Available online at www.rmme.ac.cn

Science Press

Cite this article as: Cao Hui, Wang Jingqi, Zhou Baocheng, et al. Effect of γ/α_2 Phase Interface on Supersonic Fine Particle Bombardment of TiAl Alloy by Molecular Dynamics Simulation[J]. Rare Metal Materials and Engineering, 2024, 53(02): 396-408. DOI: 10.12442/j.issn.1002-185X.20230292.

ARTICLE

Effect of γ/α_2 Phase Interface on Supersonic Fine Particle Bombardment of TiAl Alloy by Molecular Dynamics Simulation

Cao Hui[1,2], Wang Jingqi[1], Zhou Baocheng[1], Yu Zhaoliang[1], Yang Wenle[1], Li Haiyan[1,2], Liu Jianhui[1,2], Feng Ruicheng[1,2]

[1] School of Mechanical and Electrical Engineering, Lanzhou University of Technology, Lanzhou 730050, China; [2] Key Laboratory of Digital Manufacturing Technology and Application, Ministry of Education, Lanzhou University of Technology, Lanzhou 730050, China

Abstract: In order to investigate the effect of γ/α_2 phase interface on the deformation mechanism and mechanical properties of TiAl alloy during bombardment process, the supersonic fine particle bombardment of dual-phase TiAl alloy was simulated by molecular dynamics. Results show that the impact deformation mechanisms of γ/α_2 models with different thickness ratios are different, and the deformation is mainly concentrated at the γ phase and interface. With decreasing the γ phase thickness, the dislocations in contact with the phase interface are firstly absorbed by the mismatched dislocation network, then they are nucleated at the phase interface, and eventually the dislocations pass through the phase interface, entering the α_2 phase. Shockley dislocation is the main dislocation type in the impact process, and incomplete stacking fault tetrahedron forms in the specimen. After impact, uniaxial tensile simulation and nano-indentation simulation were conducted to measure the strength and surface hardness of the specimens. The main deformation mechanisms of specimens with different thickness ratios are the phase transformation, twins, and stacking faults during tensile process. Compared with other specimens, TiAl alloy with thickness ratio of 1:3 has the highest yield strength, the highest hardness, and the highest elastic modulus after impact.

Key words: molecular dynamics; phase interface; TiAl/Ti_3Al; mechanical properties; plastic deformation

TiAl alloys with lamellar layer structure are commonly used in the aerospace defense and navigation, electronic devices, and transportation industries due to their excellent comprehensive properties, including high specific strength and superb resistance against oxidation and corrosion[1–4]. It is widely reported that the dual-phase TiAl alloys have higher strength, better ductile property, and stronger resistance against corrosion, compared with the single-phase TiAl alloys[5–9]. However, the application of TiAl alloys are restricted by their low plasticity at room temperature, low fracture toughness, and rapid crack propagation rate[10–11]. The material failure mainly occurs near the surface area in engineering applications. Surface nanosizing can be accomplished by applying a thin coating of nanostructure layer to the material surface. Through the amelioration on surface and structure, the comprehensive performance and behavior are improved. Supersonic fine particle bombardment (SFPB) is a novel surface modification technique to accomplish the self-nanosizing. In SFPB process, numerous tiny solid particles with size of 0.05–200 μm[12] continually impact the metal surface at the speed of 340 m/s.

SFPB technique has been extensively employed for TiAl alloys. Wu et al[13] investigated the effect of SFPB on the fatigue properties of TC11 titanium alloy and found that the fatigue properties of TC11 alloy are significantly improved after SFPB modification. Wang et al[14] investigated the nanocrystallization mechanism and the evolution of self-nanosized grains on the Ti-6Al-4V alloy surface after SFPB. It

Received date: May 16, 2023
Foundation item: National Natural Science Foundation of China (52065036); Key Program of Natural Science Foundation of Gansu (23JRRA760); Natural Science Foundation of Gansu (22JR5RA298); Hongliu First-Class Disciplines Development Program of Lanzhou University of Technology
Corresponding author: Feng Ruicheng, Ph. D., Professor, School of Mechanical and Electrical Engineering, Lanzhou University of Technology, Lanzhou 730050, P. R. China, Tel: 0086-931-5135199, E-mail: postfeng@lut.edu.cn

is demonstrated that SFPB changes the surface microstructure of Ti-6Al-4V alloy, and the surface microhardness is significantly improved. Ge et al[15] prepared the materials with high hardness of 6272 MPa by SFPB technique. It is reported that the nanocrystalline surface layers on Ti-6Al-4V alloy have average grain size of 16 nm. Gao et al[16] studied the effect of shot peening on the microstructure of TC4 titanium alloy and found that the shot peening layer has many dislocations which are entangled with each other and deformation twins, and the twins are crucial to the plastic deformation of TC4 titanium alloy.

However, it is difficult to observe the microstructure evolution during the experiment due to the time and size restrictions. With the development of computer science and numerical simulation algorithms, molecular dynamics (MD) simulation has become a useful technique for the study of nanostructured materials. MD can simulate the atomic evolution of system and visualize the mechanism of experiment phenomena[17–19]. The dual-phase TiAl alloys have been widely investigated by MD simulation. Wei et al[20–21] calculated the fracture energies of (111) plane in γ-TiAl, (0001) plane in α_2-Ti_3Al, and γ/α_2 phase interface, which were 3.45, 3.62, and 4.03 J/m^2, respectively. Li et al[22] discussed the mechanical properties and deformation mechanisms of dual-phase TiAl alloys with γ/α_2 interfaces. It is reported that the phase interfaces can act as dislocation sources or crack sources under different boundary conditions. Chen et al[23] studied the effect of temperature on the diffusivity and mechanical properties of the nano-TiAl/Ti_3Al interface by MD simulation. Chauniyal et al[24] studied the nucleation sites of dislocations at the γ/α_2 phase interface by MD and investigated the effect of lamellar thickness on the strain of dislocation nucleation. Chen et al[25] studied the effect of temperature on the compression response and deformation mechanism of TiAl/Ti_3Al composites by MD simulation. Xiang et al[26] found that the twin boundaries and phase boundaries have a positive synergistic effect on the strength and ductility of layered TiAl single crystals through comprehensive MD simulations and theoretical analysis. Xiang et al[27] investigated the dislocation retraction of TiAl/Ti_3Al laminates by MD simulation. The theoretical model shows that the dislocation retraction occurs when the layer thickness is less than 12 nm. Moreover, the dislocation retraction after yielding is more pronounced at higher temperatures, which leads to less material failure. It can be concluded that the γ/α_2 phase interface plays an important role in the plastic deformation of materials. The phase interface not only is the origin of dislocations and twins, but also hinders the generation of dislocation slip and deformation twins. Due to the strong anisotropy of the lamellar structures in TiAl alloys, the mechanical behavior of TiAl alloys depends on the orientation, thickness, and proportion of lamellar structures. The interface type depends on the lamella thickness[28], and the yield strength of the coherent interface is higher than that of the non-coherent interface[29]. It is reported that the smaller the lamella thickness, the better the creep performance under high stress[30]. Therefore, it is necessary to investigate the influence of γ/α_2 thickness ratio on mechanical properties of TiAl alloys.

Currently, the deformation mechanism under tension/compression and the effect of temperature on the interface deformation of TiAl alloys are extensively researched. However, the deformation mechanism of TiAl alloy in SFPB process is still obscure. Through MD simulation of SFPB process, the deformation mechanism and the influence of γ/α_2 thickness ratio on the mechanical properties of TiAl alloy were investigated. This research may provide guidance for the process design of laminar structure stability to improve the TiAl alloy performance and to accelerate the practical applications.

1 Simulation Method

LAMMPS software was used to conduct MD simulations of SFPB process of TiAl alloy. In order to simulate the atomic interactions in system, Zope et al[31] employed the potential function of embedded atom method (EAM) to describe the interacting forces between metals. This research also adopted the EAM potential function to simulate the TiAl alloy[32–34].

EAM potential function expressed by the interatomic interactions can control the behavior of interatomic interactions and fundamentally determine the material properties. Therefore, the selection of potential function has a significant influence on the MD simulation results. The total potential energy in the simulated system E can be expressed, as follows:

$$E = \sum_i F_i\left[\sum_j \varphi\left(r_{ij}\right)\right] + \sum_{ij} V\left(r_{ij}\right) \quad (1)$$

where F_i is the local electron density energy; $\Sigma_j\varphi(r_{ij})$ is the amount of electron density of the atom j except atom i; $V(r_{ij})$ is the interatomic pair potential; r_{ij} is the interatomic distance.

The simulation models for the γ-TiAl phase and α_2-Ti_3Al phase were designed to satisfy the Blackburn orientation relationship of $[111]\gamma//[0111]\alpha_2$, as shown in Fig. 1. Five different models with thickness ratios of γ phase to α_2 phase as 1:1, 1:2, 1:3, 1:4, and 1:5 were established. Periodic boundary conditions were used in all directions during the simulations. To ensure accuracy, all models were relaxed at 300 K by NVE system synthesis method with time step of 0.001 fs. The atomic types and local lattice were analyzed by the common nearest neighbor method[35] in OVITO software[36]. The dislocation analysis function[37] was used to identify the microscopic defects, such as dislocations during impact and stretching processes. Due to the formation of mismatch dislocation structures, the mismatch dislocations network is formed at the γ/α_2 interface[38], and uneven forces are generated in both crystals near the interface, as shown in Fig. 2. The mismatch dislocation network at the interface reflects the significant stress concentration, especially at the nodes, as shown in Fig. 2a. Fig. 2b shows the dislocation network at the γ/α_2 interface.

The bombardment process parameters for all simulations are shown in Table 1. In this research, the γ-α_2 dual-phase TiAl

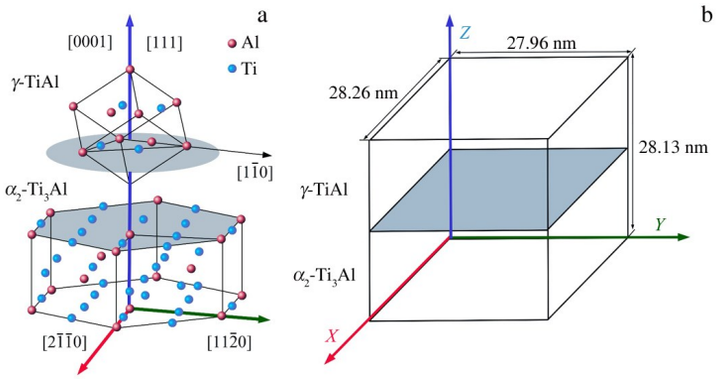

Fig.1 Schematic diagrams of crystal coordinate system (a) and γ/α_2 interface (b) of TiAl/Ti_3Al interface

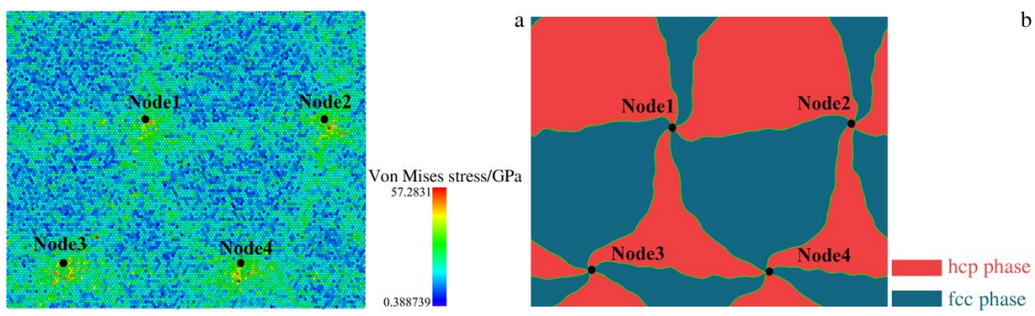

Fig.2 γ/α_2 interface structure: (a) Von Mises stress distribution and (b) dislocation line distribution

Table 1 Simulation parameters of SFPB process of dual-phase TiAl alloy

Parameter	Value
Workpiece size/nm	28.26 nm×27.96 nm×28.13
Impact speed/m·s^{-1}	4000
Impact direction	$[111]_\gamma//[0111]\alpha_2$
Initial temperature/K	300
Number of impact pellets	9 grains
Radius of impact pellets/nm	3
Number of impacts	3

alloy was used for SFPB simulation, and the impact direction was along the negative *Z*-axis direction. The simulation models with different thickness ratios are shown in Fig.3.

After SFPB, the strength and surface hardness of the specimens were measured by tensile simulations and nanoindentation simulations of TiAl alloy. The deformation stretching method was selected to perform the energy minimization in MD simulation by conjugate gradient method, followed by the equilibrium of system at isothermal isovolumetric system synthesis. The timestep was 1 ps and the uniaxial stretching was performed along *Z*-axis. Before the nanoindentation, the model was equilibrated at the micro-regular system synthesis at temperature of 300 K. The bottommost atoms were fixed as boundary atoms in the nanoindentation simulation to prevent atomic movement during the indentation process. A solid spherical indenter was used to simulate the indentation response of different models with radius of 5 nm. The indenter was moved downward at the constant speed of 50 m/s. The hardness H and elastic modulus E can be obtained from the load-displacement curves and related equations, as follows:

$$H = \frac{P_{\max}}{A_c} \tag{2}$$

$$E_r = \frac{\sqrt{\pi}}{2\beta}\frac{s}{\sqrt{A_c}} \tag{3}$$

$$A_c = \pi h(2R - h) \tag{4}$$

$$\frac{1}{E_r} = \frac{1-\upsilon^2}{E} + \frac{1-\upsilon_i^2}{E_i} \tag{5}$$

where $P_{\max}$ is the maximum load; $h_{\max}$ is the maximum displacement; s is contact stiffness; A_c is the contact area between indenter and material during indentation test; h is the displacement; β is a constant related to the indenter shape; R is radius; E_r is the approximate elastic modulus; υ is the Poisson's ratio; E_i and υ_i are the elastic modulus and Poisson's ratio of the test material i, respectively. For a spherical indenter, β =1 [39], and E_r is used to explain the elastic deformation of the specimen. With υ=0.23[40], the hardness of the diamond indenter in this research is greater than that of the test material. Therefore, E_i is infinity and υ_i=0.3.

2 Results and Discussion

2.1 Deformation mechanism of TiAl alloy with different thickness ratios

2.1.1 Mechanism of impact deformation

Atomic evolution graphs are used to analyze the

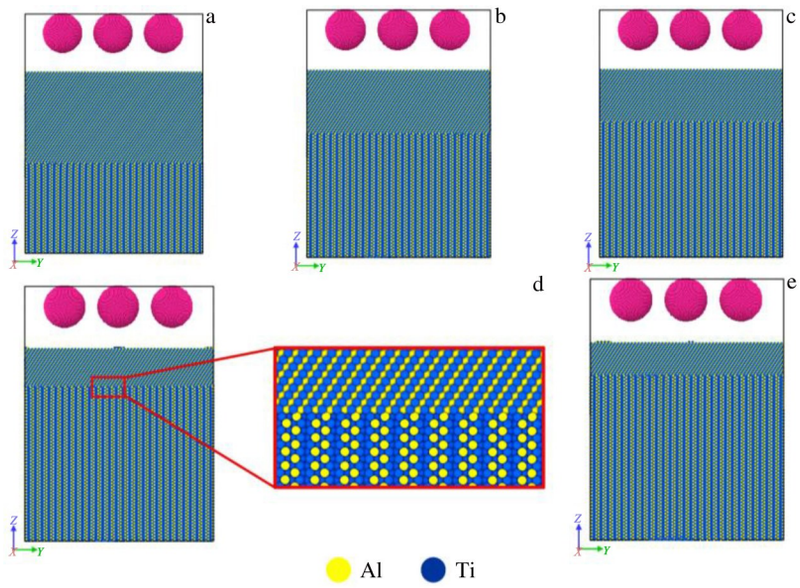

Fig.3 Schematic diagrams of SFPB models with different γ/α_2 thickness ratios: (a) 1:1, (b) 1:2, (c) 1:3, (d) 1:4, and (e) 1:5

deformation mechanism of TiAl alloys with different γ/α_2 thickness ratios under impact. Fig. 4 shows the defect evolution of the dual-phase TiAl alloy with γ/α_2 thickness ratio of 1: 1 during SFPB process. A large number of Shockley dislocations can be observed on the γ-TiAl side near the crater to release the local stress concentration, as shown in Fig. 4a. Intrinsic stacking faults (ISFs) can also be observed, and the Hirth dislocation with Burgers vectors of $1/3[\bar{1}00]$ coupled with stair-rod dislocation with Burgers vector of $1/6[\bar{1}0\bar{1}]$ is generated near ISF. The stair-rod dislocation response is as follows:

$$1/6[\bar{2}1\bar{1}]+1/6[1\bar{1}\bar{2}]\rightarrow 1/6[\bar{1}0\bar{1}] \quad (6)$$

The face-centered cubic (fcc)→body-centered cubic (bcc) and fcc→hexagonal close-packed (hcp) phase transformations occur at the surface due to the impact on γ-TiAl, which causes the atom migration. These phenomena can also be observed in other fcc materials[41]. ISFs in Fig. 4a are transformed into the extrinsic stacking faults (ESFs), as shown in Fig. 4b, which consist of hcp layer+fcc layer+hcp layer sandwich structures. ISF consists of two adjacent layers of hcp atomic surfaces. The original periodic stacking order of atoms is destroyed by the atomic plane slip caused by dislocation reactions and motions on different slip planes, resulting in two kinds of stacking faults. Shockley dislocations move along the $(\bar{1}11)$ slip surface to the phase interface by shear slip. ESFs in Fig.4b are transformed into two twins by the impact, as shown in Fig. 4c. According to Fig. 4b, two ISFs reach the phase interface and disappear. This phenomenon suggests that the Shockley dislocations reaching the phase interface are absorbed by the interface, preventing the crossing. As a result, the atoms at interface are rearranged during this absorption process.

Fig. 5 shows the defect evolution of dual-phase TiAl alloy with γ/α_2 thickness ratio of 1:2 under SFPB. Comparing Fig.5a and Fig. 4a, the stacking faults produced in the model of the dual-phase TiAl alloy with γ/α_2 thickness ratio of 1: 2 are closer to the phase interface. Additionally, incomplete stacking fault tetrahedrons (ISFTs) are generated, as shown in Fig. 5b. According to Fig. 6, the generated ISFTs collapse under impact, and the residual portion forms smaller ISFT, as shown in Fig.5c. ISFT in Fig.6a has the vertexes of A_1, k_1, k_2, and k_3, which represent Burgers vectors of $1/6[\bar{1}01]$, $1/6[0\bar{1}\bar{1}]$, and $1/6[110]$ stair-rod dislocations, respectively. Under external loading stress, dislocations are continuously generated and annihilated, and the reactions occur between dislocations. At the k_1 vertex, other dislocations can also be observed; some dislocations disappear at vertex k_3; the dislocation decomposition may occur at vertex k_2. These

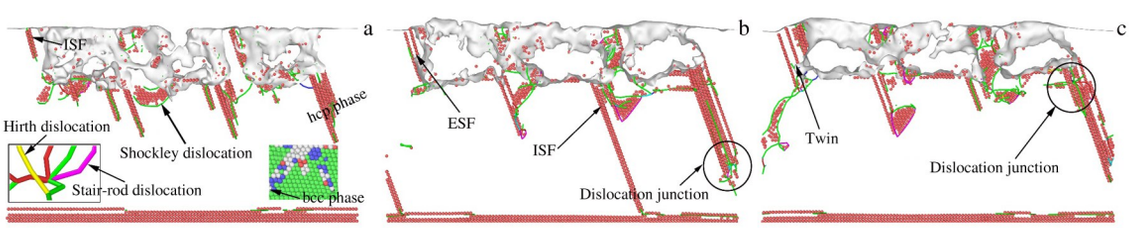

Fig.4 Defect evolution at TiAl/Ti_3Al interface on *YOZ* plane of simulation model with γ/α_2 thickness ratio of 1:1 under impact: (a) t=15 ps, (b) t= 33 ps, and (c) t=40 ps

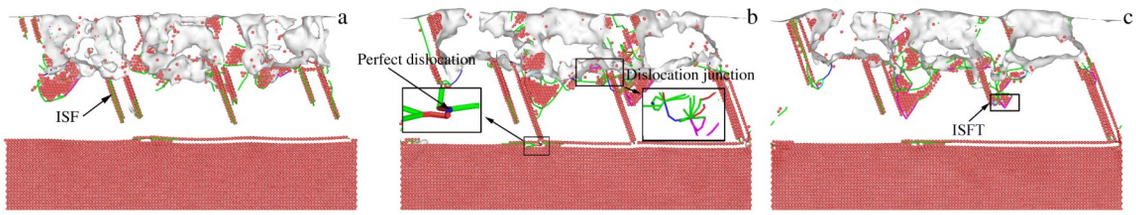

Fig.5 Defect evolution at TiAl/Ti_3Al interface on *YOZ* plane of simulation model with γ/α_2 thickness ratio of 1:2 under impact: (a) t=15 ps, (b) t=33 ps, and (c) t=40 ps

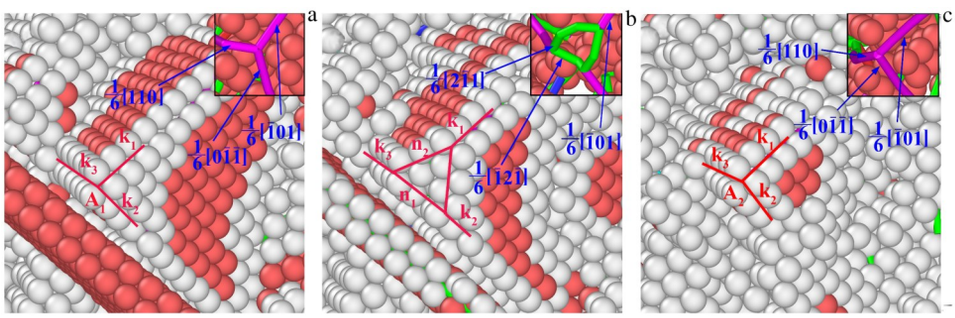

Fig.6 Evolution of ISFTs under impact

phenomena can be expressed by Eq.(7), as follows:

$$1/6[\bar{1}01] \rightarrow 1/6[\bar{2}1\bar{1}] + 1/6[1\bar{1}2] \quad (7)$$

Subsequently, the vertex A_1 collapses, as shown in Fig. 6b. With the impact further proceeding, the defects in Fig. 6b interact with the surrounding defects and smaller ISFTs are formed, as shown in Fig. 6c. This result is consistent with that in Ref.[42].

The Shockley dislocation with Burgers vector of $1/6[\bar{1}\bar{1}2]$ can be observed in Fig. 5b, which moves along the dense row surface [111] to the α_2 phase and finally reaches the phase interface. The Shockley dislocation reacts with the mismatch dislocations at the interface, thereby generating other dislocations and finally forming perfect dislocations with Burgers vector of $1/2[\bar{1}0\bar{1}]$. The thickness of the γ phase in the model with γ/α_2 thickness ratio of 1: 2 is smaller than that with the γ/α_2 thickness ratio of 1: 1. Due to the difference in thickness, dislocations can overcome the obstruction of phase interface and pass through the interface under the effect of continuous impact by the high-speed projectile. A large number of white defective atoms are produced in the α_2 phase and subsequently rearranged, as shown in Fig.5c.

Fig. 7 shows the defect evolution process of the dual-phase TiAl alloy with γ/α_2 thickness ratio of 1: 3 under SFPB. According to Fig. 7a, because the γ phase is relatively thinner, compared with that in the models with γ/α_2 thickness ratio of 1: 1 and 1: 2, the dislocations arrive at the interface firstly under the impact of high-speed projectiles. However, they cannot overcome the obstruction caused by the phase interface. Thus, the dislocation plugging occurs near the phase interface. A wave-like morphology can be observed at the phase interface, indicating that the interface migrates during the impact deformation process. By absorbing the dislocation to the migration interface, the distortion energy in the matrix is reduced. The migrated interface effectively adapts to the deformation in the lamellar structure[43]. With increasing the number of bombardments and bombardment depths, the dislocation density in the γ phase is increased dramatically and the dislocations eventually break through the phase boundary. The dislocations nucleate at the interface and slip on the column surface $\{10\bar{1}0\}$ in the α_2 phase, generating a complete dislocation with Burgers vector of $1/3[11\bar{2}0]$. Subsequently,

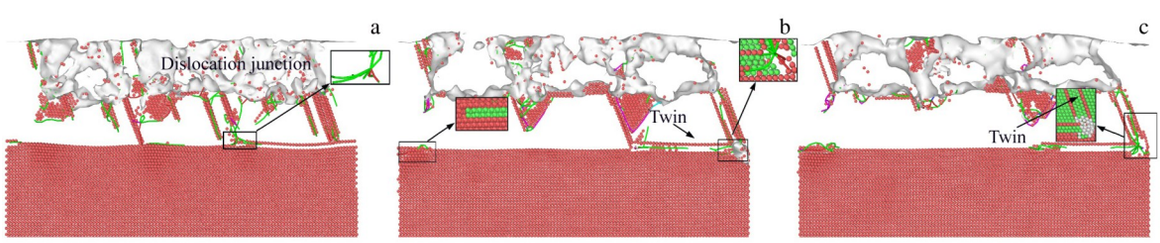

Fig.7 Defect evolution at TiAl/Ti_3Al interface on *YOZ* plane of simulation model with γ/α_2 thickness ratio of 1:3 under impact: (a) t=15 ps, (b) t=33 ps, and (c) t=40 ps

the full dislocation decomposes into two dislocations, as follows:

$$1/3[11\bar{2}0] \rightarrow 1/3[10\bar{1}0] + 1/3[01\bar{1}0] \quad (8)$$

TiAl has face-centered tetrahedron structure, which is similar to fcc structure. Ti_3Al has hcp structure, which has less slip system than the fcc structure does. When a large number of dislocations are continuously generated within the γ-TiAl, the dislocations move along the phase interface. After reaching the phase interface, most dislocations are absorbed by the phase interface, and a small portion of dislocations cross the interface and enter the α_2 phase. On the one hand, a large number of dislocations are continuously generated in γ-TiAl; on the other hand, the dislocations crossing the phase interface can hardly slip into the Ti_3Al side. As shown in Fig.7c, the dislocation plugging occurs at the phase interface, indicating that the flat phase interface gradually becomes wavy.

Fig.8 shows the defect evolution process of the dual-phase TiAl alloy with γ/α_2 thickness ratio of 1:4 under SFPB. As shown in Fig.8a, the endowment layer fault in the γ phase is in contact with the interface under impact force. The interface deforms into wave-like and step-like shapes. As shown in Fig. 8b, dislocation plugging also occurs at the interface. Subsequently, the dislocations with Burges vector of $1/3[\bar{1}010]$ in α_2 phase are produced. As shown in Fig. 8c, ESFs are generated, and the interface is gradually flattened.

Fig.9 shows the defect evolution process of the dual-phase TiAl alloy with γ/α_2 thickness ratio of 1:5 under SFPB. Since the thickness of γ phase is smaller than the projectile diameter, the projectile can directly contact the phase interface. As shown in Fig.9a, the main deformation region of the interface is directly below the projectile. Similar to the phenomena in other models, bcc phase transformation appears in the γ phase. Multiple dislocation plugging occurs at the interface and fcc phase transformation appears in the α_2 phase. As shown in Fig. 9b, the interface moves downward under the projectile impact and thus the interface shape changes to the step shape. Unlike other models, the interface does not become flat, as shown in Fig. 9c. The interface structure is severely damaged and a large number of dislocations merge into the α_2 phase, which causes the overall softening of the material.

The deformation mechanisms of TiAl alloys with different γ/α_2 thickness ratios during impact involve the fcc→bcc and fcc→hcp phase transformations, dislocation slip, stacking layer fault generation, deformation twinning, and impact-induced amorphization. The TiAl dual-phase alloy with γ/α_2 thickness ratio of 1:1 is mainly dominated by fcc→hcp and fcc →bcc phase transformations, impact-induced amorphization, and slip of stacking layer dislocations. A small number of deformation twins appear at the projectile bombardment surface, the phase interface absorbs dislocations, and the phase interface hinders the downward movement of dislocations in the γ phase during the whole impact process. The dual-phase TiAl alloy with thickness ratio of 1:2 also contains the Shockley dislocations with Burgers vector of $1/6[12\bar{1}]$, which slip along the $(1\bar{1}\bar{1})$ surface to the phase interface. The dislocations react with each other, finally breaking through the interface barrier into the α_2 phase. Although the dislocations at the phase interface are blocked, the original mismatch dislocation network structure at the interface is not destroyed. In addition to the phase transformation, deformation twinning, and impact-induced amorphization, the dual-phase TiAl alloy with γ/α_2 thickness ratio of 1:3 exhibits the deformation mechanism with more dislocation generation under high-stress impacts. The generated dislocations move towards the phase interface and react with the mismatch dislocations at the interface. As a result, the original structure of the mismatch dislocation

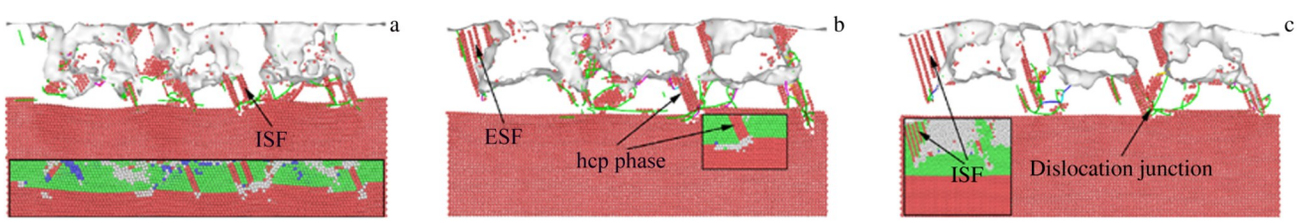

Fig.8 Defect evolution at TiAl/Ti_3Al interface on *YOZ* plane of simulation model with γ/α_2 thickness ratio of 1:4 under impact: (a) t=15 ps, (b) t=33 ps, and (c) t=40 ps

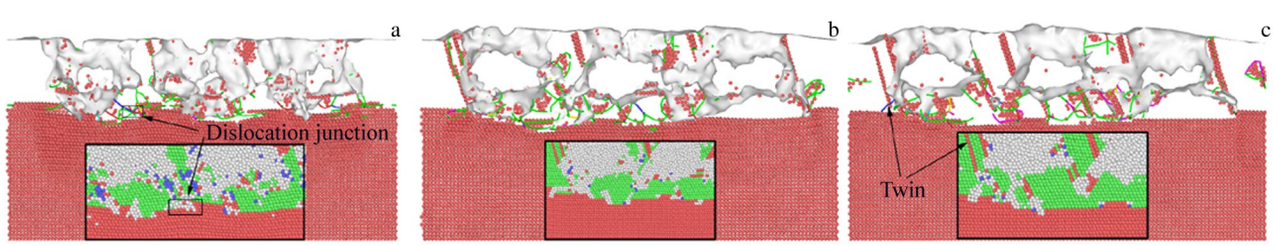

Fig.9 Defect evolution at TiAl/Ti_3Al interface on *YOZ* plane of simulation model with γ/α_2 thickness ratio of 1:5 under impact: (a) t=15 ps, (b) t=33 ps, and (c) t=40 ps

network at the interface is destroyed. To accommodate this change, the interface shape becomes wavy. The deformation mechanism of the dual-phase TiAl alloy with γ/α_2 thickness ratio of 1:4 is mainly dominated by the interfacial structure. Initially, the interface consists of wavy and stepped structures; then, the interface becomes wavy; finally, the interface flattens. The deformation mechanism of the dual-phase TiAl alloy with γ/α_2 thickness ratio of 1:5 is mainly dominated by the reactions of a large number of dislocations with the mismatched dislocation network at the interface. The interface no longer has hindrance to the dislocations. Thus, a large number of dislocations enter the α_2 phase, which causes the material softening and strength reduction. The interface cannot be restored to the flat state and presents the stepped shape.

Because dislocations are crucial to the specimen deformation and the phase interface is the main source of dislocation nucleation, different γ/α_2 thickness ratios have different dislocation densities during the impact process. The dislocation density ρ can be calculated by Eq.(9), as follows:

$$\rho = \frac{L}{V} \tag{9}$$

where L represents the total length of dislocation lines and V is the crystal volume. L can be obtained from Ovito software, and V represents the unit volume.

Fig. 10 shows the variation of dislocation density at different γ/α_2 thickness ratios. It can be seen that the Shockley dislocation density is the largest and its change is the most obvious during the impact process. As shown in Fig. 10a, the Shockley dislocation density shows upward trend before 18 ps and reaches the peak density of 8.47×10^{12} cm^{-2}. Then, the Shockley dislocation density begins to decrease after 19 ps and reaches the minimum density of 3.14×10^{12} cm^{-2} at 23 ps. This is because from 19 ps to 23 ps, under the impact of high stress, the dual-phase TiAl nucleates in the γ -TiAl and produces a large number of Shockley dislocations, which are entangled with each other. The dislocation reaction forms ISFT, which causes the increase in stair-rod dislocation density and the decrease in Shockley dislocation density. At 23 ps, the stacking faults slide along the [$\bar{1}$ 2 $\bar{1}$] direction on ($\bar{1}$ $\bar{1}$ $\bar{1}$) slip plane to the phase interface and begin to be absorbed by the interface. After 23 ps, the Shockley dislocation density increases again. This is caused by the ISFT collapse under the impact of external high stress, and ISFT decomposes into Shockley dislocations. New Shockley dislocations are also generated by impact. The stair-rod dislocation density is stable during the impact process. ISFT is generally connected to other dislocations, and complex dislocation reactions occur during impact. The densities of perfect dislocations, Frank dislocations, and Hirth dislocations increase slightly.

Fig. 10b shows the dislocation density of simulation model with γ/α_2 thickness ratio of 1: 2. It can be seen that the Shockley dislocation density reaches the peak value of 7.91×10^{12} cm^{-2} at 18 ps, which is 6.6% less than that of the simulation model with γ/α_2 thickness ratio of 1: 1. Subsequently, the Shockley dislocation density also decreases, and the lowest density of 4.294×10^{12} cm^{-2} is achieved at 30 ps, which is 36.6% higher than that of the simulation model with γ/α_2 thickness ratio of 1:1.

Fig. 10c shows the dislocation density of simulation model with γ/α_2 thickness ratio of 1: 3. It can be seen that the Shockley dislocation density has a slight increasing stage between 15 and 16 ps, and the other dislocation density increases sharply from 0.55×10^{12} cm^{-2} to 0.97×10^{12} cm^{-2}. The impact induces a large number of Shockley dislocations.

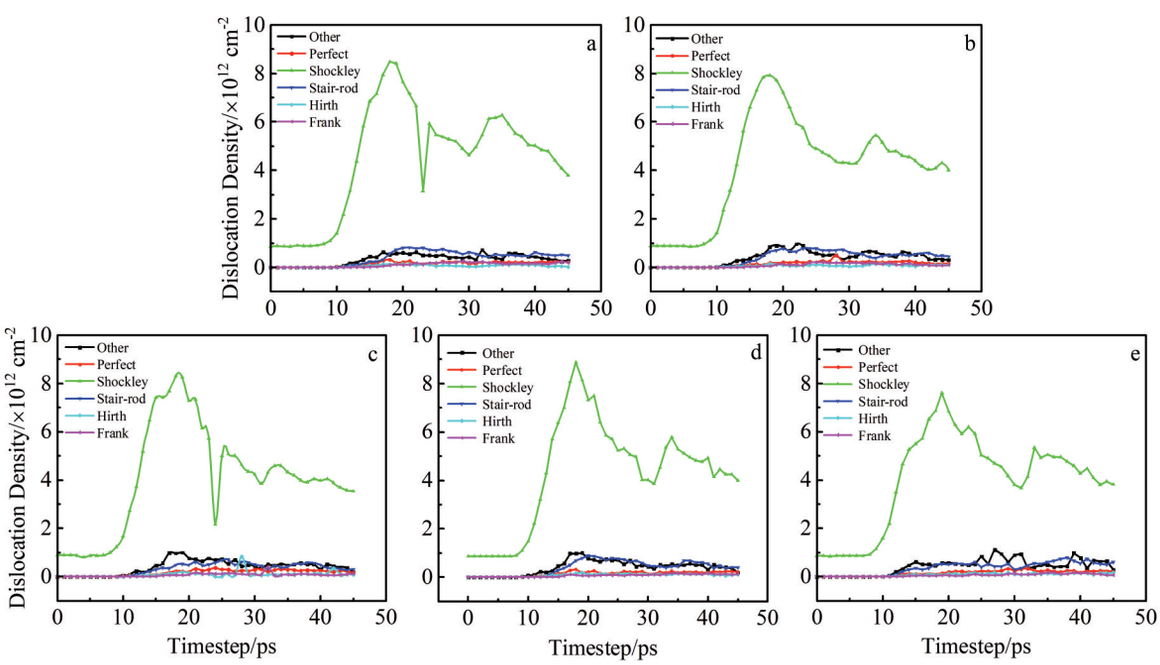

Fig.10 Dislocation densities of simulation models with γ/α_2 thickness ratio of 1:1 (a), 1:2 (b), 1:3 (c), 1:4 (d), and 1:5 (e)

However, at this time, the dislocations reach the phase interface and are absorbed by the interface. The absorbed dislocations lead to the lattice mismatch, causing the dislocations at the interface to generate other dislocations. The Shockley dislocation density reaches the peak value of 8.03×10^{12} cm^{-2} at 18 ps, and it reaches the minimum value of 2.16×10^{12} cm^{-2} at 24 ps, which is also the lowest Shockley dislocation density of all five models. When the γ/α_2 thickness ratio is 1: 3, the Shockley dislocation density does not immediately show the cliff-like decline at about 19 ps like the variation trend of other models. Instead, the Shockley dislocation density shows a step-like decline firstly, and then it rapidly declines at about 23 ps. This is because although dislocations pass through the phase interface under the impact, the hindrance of phase interface still exists. Thus, the dislocations are continuously generated at different positions of the interface, forming the dislocation pile-up phenomenon, which hinders the dislocation movement. Because the thickness of γ phase decreases, the degree of mutual reaction between Shockley dislocations increases.

Fig. 10d shows the dislocation density of simulation model with γ/α_2 thickness ratio of 1: 4. The Shockley dislocation density increases before 18 ps and reaches the peak value of 8.86×10^{12} cm^{-2} at about 18 ps. After the first shock, the mismatched dislocation network on the interface is entangled with the Shockley dislocation newly generated during the shock, and there are multiple dislocation plugs on the interface. After 15 ps, the second impact occurs, and the dislocation breaks through the interface obstruction. The Shockley dislocation density gradually decreases to 3.86×10^{12} cm^{-2} between 18 and 31 ps. Then, it rises slightly to 5.78×10^{12} cm^{-2} and becomes stable at 3.98×10^{12} cm^{-2} after the shock end. The variation trend of stair-rod dislocation density is consistent with that of Shockley dislocation density: its peak density reaches 0.89×10^{12} cm^{-2} at approximately 20 ps. This is because with increasing the number of Shockley dislocations, some Shockley dislocations react with each other, thereby forming the stair-rod dislocations. During the impact process, the density of other dislocations also changes significantly, reaching the peak value of 0.97×10^{12} cm^{-2} at 17 ps. Subsequently, other dislocations react with different dislocations and the dislocation density decreases.

Fig. 10e shows the dislocation density of simulation model with γ/α_2 thickness ratio of 1: 5. The maximum Shockley dislocation density is 7.60×10^{12} cm^{-2} at 19 ps, which is the lowest peak density of Shockley dislocations among all five models. Subsequently, the Shockley dislocation density reaches the minimum value of 3.68×10^{12} cm^{-2} at 31 ps. When the dislocations in the γ phase pass through the interface barrier, the formation of other dislocations in the α_2 phase results in the density of other dislocations to reach the peak value of 1.11×10^{12} cm^{-2} at 27 ps.

The total dislocation density in the matrix with the γ/α_2 thickness ratio of 1:1, 1:2, 1:3, 1:4, and 1:5 is 4.88×10^{12}, 5.14×10^{12}, 4.39×10^{12}, 5.39×10^{12}, and 5.15×10^{12} cm^{-2}, respectively. The matrix with γ/α_2 thickness ratio of 1:3 has the lowest total dislocation density, and the matrix with γ/α_2 thickness ratio of 1:4 has the highest total dislocation density.

2.1.2 Deformation mechanism during tensile process

During the stretching along the direction perpendicular to the interface, the crack nucleation and fracture behavior were analyzed under different dual-phase thickness ratios. The dislocations on the interface become obviously denser, and the shape of dislocation network also changes. The perfect dislocations with Burgers vector of $1/2[10\bar{1}]$ disappear, and the dislocations in the γ phase react with the dislocation at the interface, thereby forming other dislocations. Finally, other dislocations are transformed into Shockley dislocations. Then, the Shockley dislocations pass through the phase boundary and expand the α_2 phase to generate $1/3[1\bar{1}00]$ partial dislocations. The phase transformation occurs on one side of the γ phase, leading to the formation of multiple twins. Dislocation entanglement then occurs in the γ phase, gradually increasing the internal stress at the entanglement point. Eventually, the cracks nucleate at this point, as shown in Fig.11b. The ISF in Fig.11a is transformed into ESF under the tensile load, and then the extrinsic faults reach the interface and expand to the α_2 phase. The cracks are blunted with continuous stretching, forming holes. In α_2-Ti_3Al, a large number of stacking faults are produced, as shown in Fig. 11c. The pores gradually expand. Finally, the fracture occurs at the stress concentration position in the γ phase, as shown in Fig.11d.

Fig. 12 shows the crystal structure evolution on *YOZ* plane of the dual-phase TiAl alloy with γ/α_2 thickness ratio of 1: 2 during stretching deformation. The fcc→hcp phase

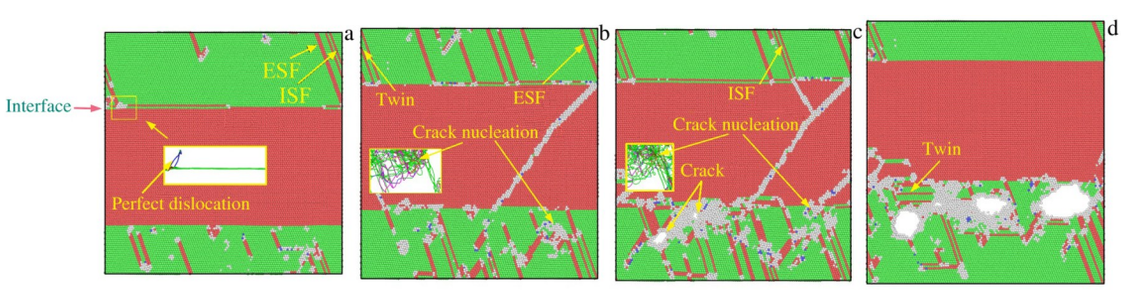

Fig.11 Crystal structure evolution on *YOZ* plane of dual-phase TiAl alloy with γ/α_2 thickness ratio of 1: 1 during stretching deformation: (a) ε=3.49%, (b) ε=5.48%, (c) ε=7.47%, and (d) ε=8.46%

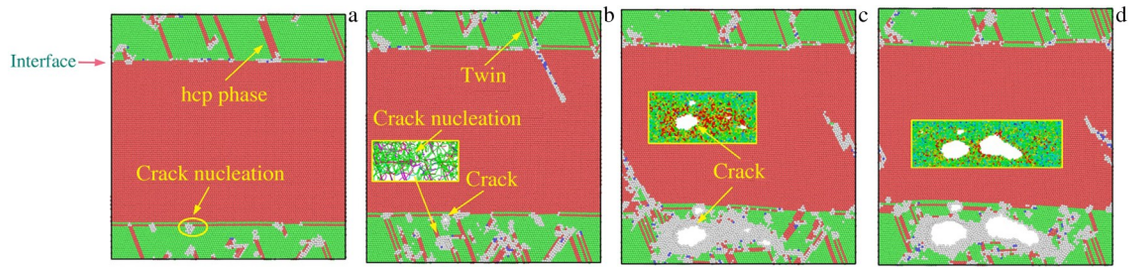

Fig.12 Crystal structure evolution on *YOZ* plane of dual-phase TiAl alloy with γ/α_2 thickness ratio of 1:2 during stretching deformation: (a) ε=3.79%, (b) ε=5.80%, (c) ε=7.80%, and (d) ε=8.80%

transformation near the interface in the γ phase is shown in Fig. 12a. Two twins are formed due to this phase transformation during the stretching process, and the dislocations with Burgers vector of $1/3[1\bar{1}00]$ are generated in the α_2 phase. As shown in Fig. 12b, under the action of external tensile force, dislocations at the interface continue to accumulate. In order to reduce the stress at interface, the interface shapes in Fig. 12b and 12c change from flat state to the stepped state. As shown in Fig. 12b–12d, the new cracks nucleate, the holes are formed, and the fracture occurs, respectively. Similar to those in the dual-phase TiAl alloy with γ/α_2 thickness ratio of 1:1, the fracture sites are all inside the γ phase.

Fig. 13 shows the crystal structure evolution on *YOZ* plane of the dual-phase TiAl alloy with γ/α_2 thickness ratio of 1:3 during stretching deformation. Fig. 13a shows that ISFT and stacking faults are the two primary forms of matrix dislocations, and twin is created at the interface. The interface changes slightly from flat shape to step-like shape in order to alleviate the tensile stress concentration, and the more severe the stretching deformation, the more obvious the shape change. Under the influence of tension, the stacking faults in γ phase slide and they are split into twins. It is reported that the conical bedding defects are formed and the hcp→bcc phase transformation occurs during additional stretching process[44]. As shown in Fig.13b, the cracks are firstly formed at the phase interface and within the phase. The crack nucleation point at the phase contact area is firstly passivated, thereby creating holes. Fig. 13c and 13d show the final fracture after hole appearance in the phase.

Fig. 14 shows the crystal structure evolution on *YOZ* plane of the dual-phase TiAl alloy with γ/α_2 thickness ratio of 1:4 during stretching deformation. Due to the strong plastic deformation at the crater, a large number of Shockley dislocations and stair-rod dislocations are entangled. Therefore, the crack nucleation locations during the stretching

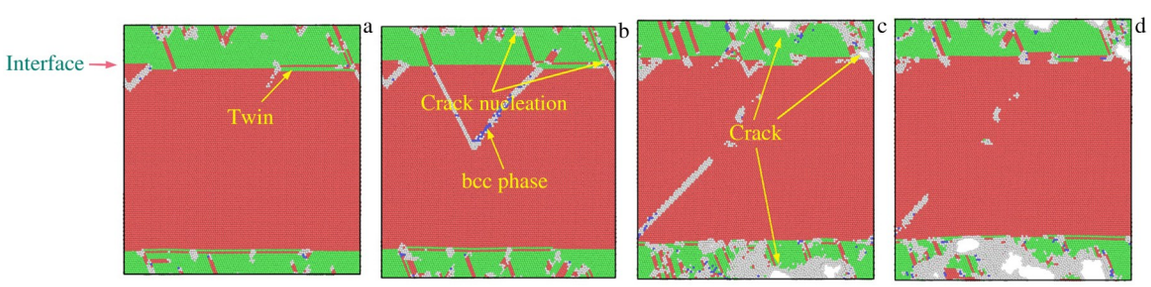

Fig.13 Crystal structure evolution on *YOZ* plane of dual-phase TiAl alloy with γ/α_2 thickness ratio of 1:3 during stretching deformation: (a) ε=4.03%, (b) ε=6.03%, (c) ε=8.04%, and (d) ε=9.04%

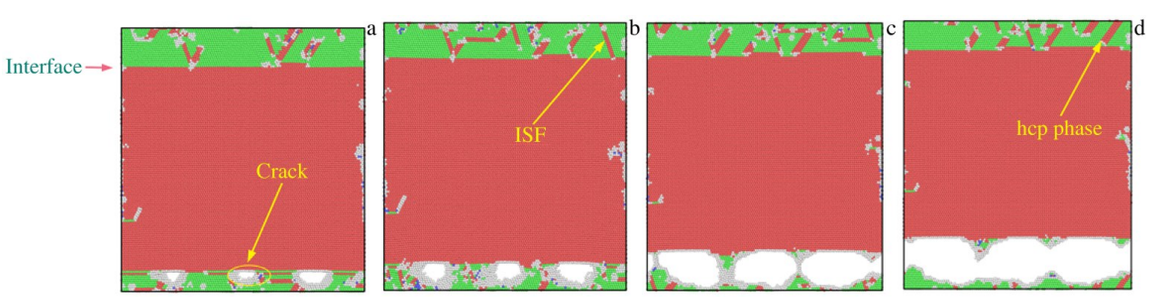

Fig.14 Crystal structure evolution on *YOZ* plane of dual-phase TiAl alloy with γ/α_2 thickness ratio of 1:4 during stretching deformation: (a) ε=0.81%, (b) ε=2.78%, (c) ε=5.72%, and (d) ε=9.65%

process are concentrated near the residual craters within the matrix after the impact. It is observed that ISFs appear near the surface in the γ phase when the strain is 0.81%, as shown in Fig. 14a. Cracks are formed and then passivated, thereby producing three holes. Then, the holes gradually expand, and the Shockley dislocations with Burges vector of $1/6[11\bar{2}]$ slide along the (111) compact plane to the interface, as shown in Fig. 14b. Subsequently, the holes further expand, as shown in Fig. 14c. Finally, the fracture occurs within the γ phase at strain of 9.65%, as shown in Fig.14d.

Fig. 15 shows the crystal structure evolution on *YOZ* plane of the dual-phase TiAl alloy with γ/α_2 thickness ratio of 1∶5 during stretching deformation. As shown in Fig. 15a, due to the thin thickness of γ lamella phase, the material is softened after impact, and the cracks appear at the strain of 0.46%. As shown in Fig. 15b and 15c, the crack gradually expands. Finally, the structure breaks in the γ phase, as shown in Fig.15d.

The crack nucleation mechanism of the TiAl alloys with different γ/α_2 thickness ratios during the tensile stretching process was compared and analyzed. It can be concluded that the crack nucleation position of the dual-phase TiAl alloys changes with the variation of thickness ratio. When the γ/α_2 thickness ratio is 1∶1, the crack nucleation location is primarily within the γ phase. When the γ/α_2 thickness ratio is 1∶2, the crack nucleation location is primarily within the γ phase, and some cracks are formed on the interface. When the γ/α_2 thickness ratio is 1∶3, cracks can mainly be observed within the γ phase and at the phase interface. The crack extension occurs at the interface. When the γ/α_2 thickness ratio is 1∶4, the crack nucleation location is concentrated near the residual crater in the matrix after impact. Due to the thin thickness of γ lamella phase, the material is softened after impact, and the TiAl alloy with γ/α_2 thickness ratio of 1∶5 breaks firstly.

2.2 Mechanical properties

To investigate the effect of γ/α_2 thickness ratio on the mechanical properties of TiAl alloys after impact and the effect of phase boundary strengthening, the γ-TiAl alloys and dual-phase TiAl alloys with different γ/α_2 thickness ratios were uniaxially stretched along *Z*-direction.

Fig. 16 shows the tensile stress-tensile strain curves of the γ-TiAl alloy and dual-phase TiAl alloys with different γ/α_2 thickness ratios, and Fig. 17 shows the relationship between yield stress and thickness ratio of the γ-TiAl alloy and dual-phase TiAl alloys with different γ/α_2 thickness ratios. According to Fig. 16, the γ-TiAl alloy yields at the tensile strain of 2.47% and the yield strength is 2.55 GPa. The dual-phase TiAl with γ/α_2 thickness ratio of 1∶1 yields at strain of 5.92% and its yield strength is 5.41 GPa, which is 2.12 times higher than that of γ-TiAl alloy. The dual-phase TiAl with γ/α_2 thickness ratio of 1∶2 yields at strain of 6.8% and its yield strength is 5.48 GPa, which is 2.14 times higher than of that of γ-TiAl alloy. The dupl-phase TiAl with γ/α_2 thickness ratio of 1∶3 yields at strain of 7.03% and its yield strength is 5.51 GPa, which is 2.16 times higher than that of γ-TiAl alloy. The phase boundary can increase the yield strength of materials. It is observed that the maximum tensile stress of the dual-phase TiAl alloy with γ/α_2 thickness ratio of 1∶3 is basically the same as that with γ/α_2 thickness ratio of 1∶2. However, the maximum tensile stress of the dual-phase TiAl alloy with γ/α_2 thickness ratio of 1∶3 is about 2% higher than that with γ/α_2 thickness ratio of 1∶1. With changing the γ/α_2 thickness ratio from 1∶1 to 1∶3, the yield strength is increased slightly. When the γ/α_2 thickness ratio is 1∶4 and 1∶5, the yield strength decreases. The yield strength of dual-phase TiAl alloys with different thickness ratios is always higher than that of γ-TiAl alloy. Thus, it is clear that the phase boundary can enhance the yield strength of material, which is consistent with the experiment results in Ref.[45].

Nanoindentation simulations along *Z*-axis were conducted on the machined specimens, and the hardness and elastic modulus were calculated from the displacement-load curves. Fig. 18 shows the load-displacement curves during the nanoindentation process. It can be seen that the whole indentation process includes two stages: loading and unloading. Negative load indicates the existence of an attractive force between the specimen and the indenter, and positive load indicates the existence of pressure between the specimen and the indenter. The indentation process can be divided into three stages. The first stage: the indenter gets close to the material; the second stage: the indenter is pressed into the material; the third stage: unloading. During the second stgae, there is pressure between the indenter and the material, and the load is increased with increasing the displacement depth. In the third stage, when the indenter

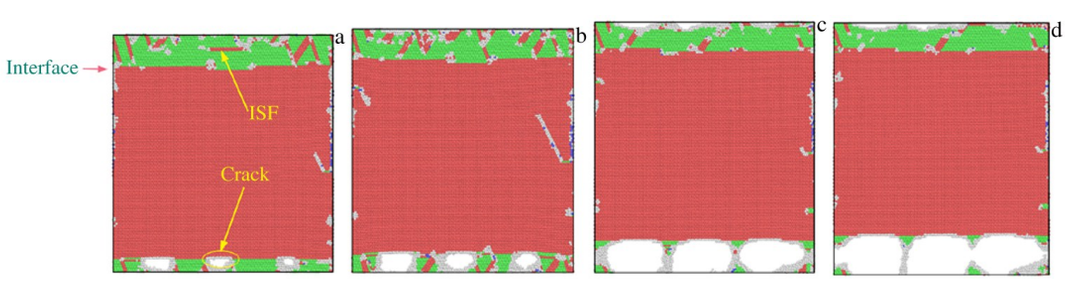

Fig.15 Crystal structure evolution on *YOZ* plane of dual-phase TiAl alloy with γ/α_2 thickness ratio of 1∶5 during stretching deformation: (a) ε=0.46%, (b) ε=2.92%, (c) ε=6.85%, and (d) ε=9.80%

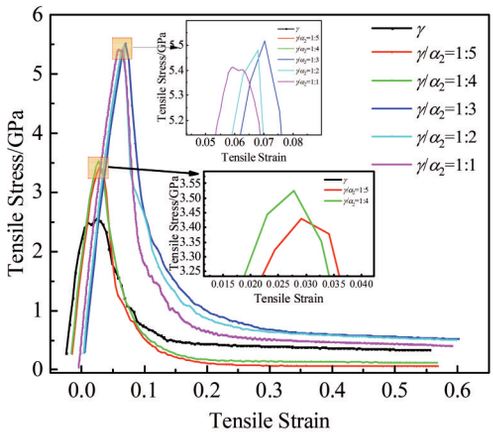

Fig.16 Tensile stress-tensile strain curves of simulation models of γ-TiAl alloy and dual-phase TiAl alloys with different γ/α_2 thickness ratios after SFPB process

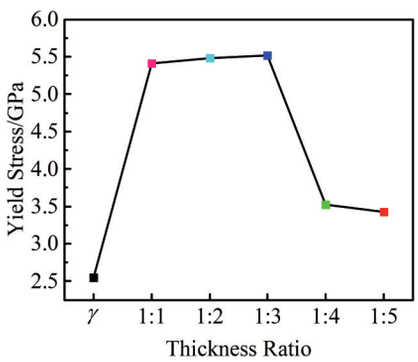

Fig.17 Relationship between yield stress and thickness ratio of γ-TiAl alloy and dual-phase TiAl alloys with different γ/α_2 thickness ratios

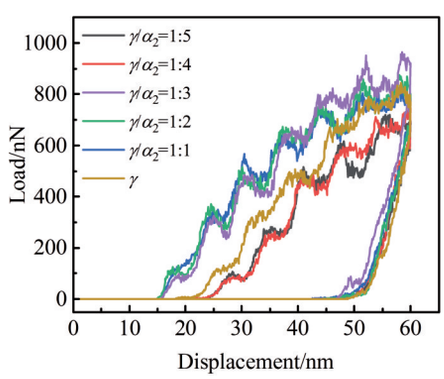

Fig.18 Load-displacement curves of γ-TiAl alloy and dual-phase TiAl alloys with different γ/α_2 thickness ratios

reaches the maximum depth, the indenter starts to withdraw to the initial position, and the load gradually decreases to nearly 0. It can be observed that the load of TiAl alloy with γ/α_2 thickness ratios of 1:3 is the maximum, whereas that with γ/α_2 thickness ratios of 1:5 is the minimum.

The elastic modulus and hardness can be calculated by Eq.(2–5), and the results are shown in Fig.19. Both the elastic modulus and hardness are changed with varying the γ/α_2 thickness ratio, and these two parameters show the basically same variation trend. The maximum hardness and elastic modulus can be achieved for the dual-phase TiAl alloy with γ/α_2 thickness ratio of 1: 3, and the minimum hardness and elastic modulus can be achieved for the dual-phase TiAl alloy with γ/α_2 thickness ratio of 1:5. The elastic modulus and hardness are increased firstly and then decreased with changing the γ/α_2 thickness ratio from 1: 1 to 1: 5, and the critical lamella size of γ phase is approximately 7 nm. When the lamella thickness λ is greater than 7 nm, the hardness of dual-phase TiAl alloys is increased with decreasing the lamella thickness, according to the Hall-Petch relationship. Based on the abovementioned analysis, it can be concluded that the dislocation accumulation in γ phase is mainly caused by the obstruction of phase boundary, and a few dislocations pass through the phase boundary, which leads to the hardening of material. When the thickness of γ phase is less than 7 nm, a large number of dislocations pass through the phase boundary due to the destruction of the mismatch dislocation network structure at the interface, resulting in the softening phenomenon. The material hardness is decreased with increasing the γ phase thickness, according to the inverse Hall-Petch relationship[46]. By comparing the strength and hardness of dual-phase TiAl alloys with different thickness ratios, it is clear that TiAl alloy with γ/α_2 thickness ratio of 1: 3 has the optimal mechanical properties after impact.

Although certain results are obtained in this research, some shortcomings or limitations still exist. Thus, the further research should focus on the number of projectiles and the number and time of impact in the simulation, which are related to the mechanical response of the material after impact. These factors should be considered in the simulation. Although the effect of thickness ratio on the mechanical properties of dual-phase TiAl alloys after bombardment was analyzed in this research, many other factors should also be considered in the actual processing.

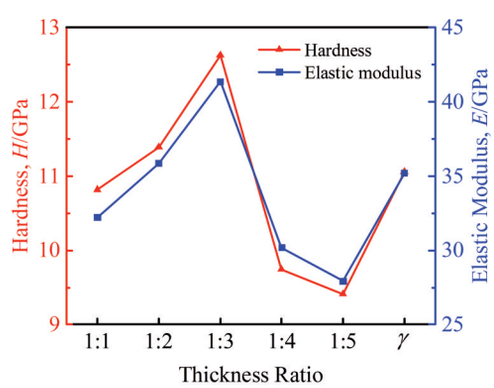

Fig.19 Hardness and elastic modulus of γ-TiAl alloy and dual-phase TiAl alloys with different γ/α_2 thickness ratios

3 Conclusions

1) The deformation mechanisms of dual-phase TiAl alloys with different γ/α_2 thickness ratios during the impact process are mainly the transformation of face-centered cubic phase→ hexagonal close-packed phase, face-centered cubic phase→ body-centered cubic phase, dislocation slip, laminated fault formation, deformation twins, and impact-induced amorphous phase.

2) The Shockley dislocations are in the dominant position during the impact. After the impact, the dislocation density of dual-phase TiAl alloy with γ/α_2 thickness ratio of 1∶4 is the highest, and that of the dual-phase TiAl alloy with γ/α_2 thickness ratio of 1:3 is the lowest.

3) Under uniaxial tension, the crack nucleation occurs in the γ phase of dual-phase TiAl alloy with different γ/α_2 thickness ratios, but the nucleation positions are different. The cracks in the dual-phase TiAl alloy with γ/α_2 thickness ratio of 1∶3 nucleate not only in the γ phase but also at the interface, and the crack propagation proceeds simultaneously at these two places.

4) The strength, hardness, and elastic modulus of the dual-phase TiAl alloy with γ/α_2 thickness ratio of 1∶ 3 are the highest, according to the Hall-Petch effect. The existence of the phase boundary greatly improves the yield stress of the material, and the variation trends of hardness and elastic modulus are consistent.

References

1 Appel F, Clemens H, Fischer F D. *Progress in Materials Science*[J], 2016, 81: 55

2 Jiao Y, Huang L J, Wei S L *et al. Corrosion Science*[J], 2018, 140: 223

3 Klein T, Usategui L, Rashkova B *et al. Acta Materialia*[J], 2017, 128: 440

4 Duan B H, Yang Y C, He S Y *et al. Journal of Alloys and Compounds*[J], 2022, 909: 164811

5 Marketz W T, Fischer F D, Clemens H. *International Journal of Plasticity*[J], 2003, 19(3): 281

6 Wang D P, Chen G, Wang A D *et al. International Journal of Minerals, Metallurgy and Materials*[J], 2023, 30(4): 689

7 Morris M A. *Philosophical Magazine A*[J], 1993, 68(2): 237

8 Iqbal F, Pyczak F, Neumeier S *et al. Materials Science and Engineering A*[J], 2017, 689: 11

9 Li Z P, Luo L S, Su Y Q *et al. Materials Science and Engineering A*[J], 2022, 857: 144078

10 Zhai W G, Wang P, Ng F L *et al. Composites Part B: Engineering*[J], 2021, 207: 108587

11 Hao Y J, Liu J X, Li S K. *Materials Science and Engineering A*[J], 2017, 705: 210

12 Ba D M, Ma S N, Meng F J *et al. Key Engineering Materials*[J], 2008, 373–374: 811

13 Wu Y L, Xiong Y, Liu W *et al. Surface and Coatings Technology*[J], 2021, 421: 127473

14 Wang Min, Lin Chengxiao, Ma Caixia. *Chinese Journal of Rare Metals*[J], 2011, 35(5): 633 (in Chinese)

15 Ge L L, Tian N, Lu Z X *et al. Applied Surface Science*[J], 2013, 286: 412

16 Gao Yukui. *Rare Metal Materials and Engineering*[J], 2010, 39(9): 1536 (in Chinese)

17 Au S K, Beck J L. *Structural Safety*[J], 1999, 21(2): 135

18 Walton O R. *International Journal of Engineering Science*[J], 1984, 22(8–10): 1097

19 Hollingsworth S A, Dror R O. *Neuron*[J], 2018, 99(6): 1129

20 Wei Y, Zhou H B, Zhang Y *et al. Journal of Physics: Condensed Matter*[J], 2011, 23(22): 225504

21 Wei Y, Zhang Y, Zhou H B *et al. Intermetallics*[J], 2012, 22: 41

22 Li W, Yin Y J, Xu Q *et al. Computational Materials Science*[J], 2019, 159: 397

23 Chen J S, Chen W J, Wang C H. *Applied Physics A*[J], 2020, 126: 493

24 Chauniyal A, Rebecca J. *Materials Science and Engineering A*[J], 2020, 796: 140053

25 Chen Y, Li J, Liu B *et al. Intermetallics*[J], 2022, 150: 107 685

26 Xiang H G, Guo W L. *International Journal of Plasticity*[J], 2022, 150: 103197

27 Xiang H G, Guo W L. *Science China: Physics, Mechanics & Astronomy*[J], 2021, 64(6): 264611

28 Hazzledine P M. *Intermetallics*[J], 1998, 6(7–8): 673

29 Maruyama K, Tabata A, Toriyama Y *et al. Journal of Physics: Conference Series*[J], 2010, 240: 12101

30 Wang Q, Chen R R, Yang Y H *et al. Materials Science and Engineering A*[J], 2018, 711: 508

31 Zope R R, Mishin Y. *Physical Review B*[J], 2003, 68(2): 24102

32 Ji Z W, Lu S, Hu Q M *et al. Acta Materialia*[J], 2018, 144: 835

33 Xie Z C, Gao T H, Guo X T *et al. Computational Materials Science*[J], 2015, 98: 245

34 Li P T, Yang Y Q, Xia Z H *et al. RSC Advances*[J], 2017, 7(76): 48315

35 Schiøtz J, Di Tolla F D, Jacobsen K W. *Nature*[J], 1998, 391(6667): 561

36 Stukowski A. *Modelling and Simulation in Materials Science and Engineering*[J], 2009, 18(1): 15012

37 Stukowski A. *Modelling and Simulation in Materials Science and Engineering*[J], 2012, 20(4): 45021

38 Shen C, Wang Y. *Acta Materialia*[J], 2003, 51(9): 2595

39 Chen Z W, Wang X, Bhakhri V *et al. Acta Materialia*[J], 2013, 61(15): 5720

40 He Y, Schwarz R B, Miglior A. *Journal of Materials Research*[J], 1995, 10(5): 1187

41 Qi Y M, Zhao M, Feng M L. *Journal of Alloys and Compounds*[J], 2021, 851: 156923

42 Xiong Y N, Hu W Y, Shu Y *et al. Journal of Alloys and Compounds*[J], 2022, 901: 163664

43 Zhao L R, Tangri K. *Philosophical Magazine A*[J], 1992, 65(5): 1065

44 Maurya S K, Nie J F, Alankar A. *Computational Materials Science*[J], 2021, 192: 110329

45 Huang S C. *Metallurgical Transactions A*[J], 1992, 23: 375

46 Liu Xinghua, Rui Zhiyuan, Fu Rong *et al. Rare Metal Materials and Engineering*[J], 2022, 51(2): 629 (in Chinese)

γ/α_2相界面对TiAl合金超音速微粒轰击影响的分子动力学模拟

曹　卉[1,2]，王靖淇[1]，周宝成[1]，俞兆亮[1]，杨文乐[1]，李海燕[1,2]，刘俭辉[1,2]，冯瑞成[1,2]

(1. 兰州理工大学 机电工程学院，甘肃 兰州 730050)

(2. 兰州理工大学 数字制造技术与应用教育部重点实验室，甘肃 兰州 730050)

摘　要：为探究γ/α_2相界面对TiAl合金在轰击过程中的变形机制和轰击后力学性能的影响，通过分子动力学来模拟超音速微粒轰击双相TiAl合金的过程。结果表明：γ/α_2不同厚度比模型的冲击变形机制不同，变形主要集中在γ相和界面处。随着γ相厚度的减小，与相界面接触的位错首先被界面处的失配位错网络吸收，然后在相界面处成核，最终穿过相界面进入α_2相。冲击过程中产生的位错以Shockley位错为主，试样中形成了不完全层错四面体。冲击之后分别使用单轴拉伸模拟和纳米压痕模拟，测定了试样的强度和表面硬度。拉伸过程中相变、孪晶和层错是不同厚度比试样的主要变形机制。与其他试样相比，厚度比为1:3的双相TiAl合金在冲击后具有最高的屈服强度、硬度和弹性模量。

关键词：分子动力学；相界面；TiAl/Ti_3Al；力学性能；塑性变形

作者简介：曹　卉，女，1988年生，博士，讲师，兰州理工大学机电工程学院，甘肃 兰州 730050，电话：0931-5135199，E-mail：caoh@lut.edu.cn